FULL PAPER

Modification of Carbon Nanofibres for the Immobilization of Metal Complexes: A Case Study with Rhodium and Anthranilic Acid

T. G. Ros, A. J. van Dillen, J. W. Geus, and D. C. Koningsberger*[a]

Abstract: The immobilisation of the rhodium/anthranilic acid complex onto fishbone carbon nanofibres (CNFs) was executed by means of the following steps: 1) surface oxidation of the fibres, 2) conversion of the oxygen-containing surface groups into acid chloride groups, 3) attachment of anthranilic acid and 4) complexation of rhodium by the attached anthranilic acid. The immobilisation process was followed and the resulting surface species were characterised by IR, X-ray absorption fine structure (XAFS) and X-ray photoelectron spectroscopy (XPS), and by molecular modelling. Anthranilic acid bonds to the CNFs by an amide linkage to the carboxyl groups that are present after surface oxidation of the fibres. The immobilised anthranilic acid coordinates to rhodium through the nitrogen atom and the carboxyl group. The as-synthesised Rh^{III} complex itself is not active in the liquid-phase hydrogenation of cyclohexene. Reduction with sodium borohydride yields small particles ($d = 1.5 - 2$ nm) of rhodium metal that are highly active. The results indicate that different activation procedures for the immobilised Rh/anthranilic acid system should be applied, such as reduction with a milder reducing agent or direct complexation of the rhodium in the Rh^I state.

Introduction

The immobilisation of homogeneous catalysts onto solid supports has been studied extensively since the 1970s.[1–4] The objective is to combine the advantages of homogeneous catalysts, such as a high selectivity and metal efficiency, with the simple recovery of the catalyst. A number of immobilisation methods can be distinguished, such as encapsulation or entrapment, supported liquid phase, and immobilisation by covalent bonding.

In general, immobilisation by covalent bonding ("immobilisation") of homogeneous hydrogenation catalysts is executed by first attaching one ligand to the support. This ligand is usually the most important ligand, for example, a bulky bidentate ligand that causes the immobilised catalyst to be enantioselective. Next, the metal complex is coordinated to the immobilised ligand by a ligand-exchange reaction. Other immobilisation procedures are used as well, such as reaction of a metal salt with the immobilised ligand, which may be followed by a further coordination of other ligands to the metal atom, and direct reaction of the metal centre with a surface atom of the support. Most immobilisation techniques try to maintain the structure of the immobilised catalyst as close as possible to that of its homogeneous precursor. The first 15 years of research into immobilisation have demonstrated that simple immobilisation of a successful homogeneously active, metal-complex catalyst to a functionalised support generally yields an inferior version of the homogeneous catalyst.[2] However, it has also been shown that by careful design, supported metal-complex catalysts can be prepared that have advantages not exhibited in homogeneous catalysis. Although some of the immobilised metal-complex catalysts have properties that are as good or even better than their homogeneous counterparts, in 1998 none had an industrial application.[4] This is correlated to the frequent observation of significant metal leaching, although other important factors, such as the mechanical and macroscopic properties of the support, are also decisive. The problem of leaching is often directly related to the mechanism of the catalytic reaction. For instance, immobilised phosphine-containing metal complexes will leach under hydrogenation conditions, because during catalysis one phosphine ligand must desorb to allow the required coordination of the olefin. This problem can sometimes be circumvented by the use of multi-dentate ligands.

An alternative approach could be to change the electronic and steric features of the complex by immobilisation. This approach has been exemplified by Holy, who studied the immobilisation of rhodium N-phenyl anthranilic acid

[a] Prof. D. C. Koningsberger, Dr. T. G. Ros, Dr. A. J. van Dillen,
Prof. J. W. Geus
Department in Inorganic Chemistry and Catalysis
Debye Institute, Utrecht University
P.O. box 80083, 3508 TB Utrecht (The Netherlands)
Fax: (+31) 30-2511027
E-mail: d.c.koningsberger@chem.uu.nl

(RhPAA) and rhodium anthranilic acid (RhAA) onto polystyrene.[5–7] The DMF-soluble (DMF = *N,N*-dimethylformamide) Rh^I complex of *N*-phenyl anthranilic acid (PAA) was

PAA

AA
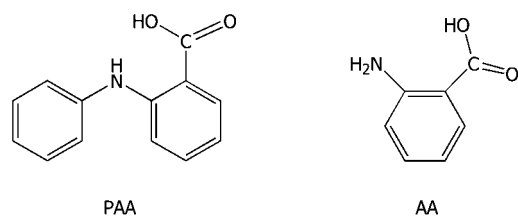
known as a remarkably active hydrogenation catalyst.[8–11] However, upon immobilisation onto polystyrene, the catalyst no longer displayed any activity. In contrast, when anthranilic acid was immobilised, a highly active Rh^I catalyst was obtained after reduction of the metal complex with NaBH$_4$. Monovalent rhodium is able to participate in the oxidative addition/reductive elimination cycle that is required to catalyse hydrogenation reactions. The rhodium/anthranilic acid complex was not known as a homogeneous catalyst. In addition, the immobilised complex of anthranilic acid with nickel showed hydrogenation activity.[12] This example demonstrates that the catalytic properties of immobilised complexes often differ from those of their non-supported counterparts. Therefore, the best approach could be to design immobilised catalysts that do not have homogeneous analogues. A weak ligand in solution, for example, an amine ligand, which may easily dissociate from the metal to result in the reduction of the metal under hydrogenation conditions, could be a suitable ligand for an immobilised system.

Although the Rh/anthranilic acid complex has been successfully immobilised on polystyrene, the relatively low thermal and mechanical stability, the swelling properties and the microporous structure of the polystyrene support complicate the use of the catalyst in an industrial environment. Carbon nanofibres (CNFs), on the other hand, are mechanically very strong and have a macroporous structure. The hydrophobicity of the fibres can be modified by surface oxidation.[13] Furthermore, the CNFs obtained after synthesis are very pure and can be grown at low cost.[14] These advantages make the CNFs a suitable support for catalytic reactions in the liquid phase. Consequently, we decided to immobilise RhAA onto fishbone-type carbon nanofibres.

To the best of our knowledge, the immobilisation (i.e., by covalent bonding) of metal complexes onto carbon nanofibres or carbon nanotubes has not yet been explored. Some reports describe the impregnation or adsorption of homogeneous catalysts on these new carbon materials.[15–17] Moreover, only few articles have been published regarding the immobilisation of metal complexes on carbon in general. Kagan et al.[18] synthesised a chiral rhodium catalyst on partially graphitised carbon, while McCabe and Orchin[19] attached cobalt and tin complexes to bituminous coal. The inertness of CNFs and, to a lesser extent, of carbon in general makes immobilisation with these materials much more difficult than with polymers or oxidic supports, such as silica or alumina. However, already in the 1970s, Miller and co-workers[20] modified graphite electrodes for the attachment of amines onto their surface. The

electrodes were kept at a high temperature in air, the resulting carboxyl groups were converted into acid chloride groups by the action of thionyl chloride, and these groups were subsequently treated with an amine. The approach of Miller has been used by several other researchers for the attachment of molecules or even metal–ligand systems to carbon electrodes, although the experimental conditions for oxidation and attachment of amine varied considerably.[21–24] Smalley and co-workers[25] and, more importantly, Haddon and co-workers[26, 27] employed the method of converting carboxyl groups on carbons to acid chloride groups and subsequent attachment of amines to shortened single-walled carbon nanotubes (SWNTs). Haddon et al. used this procedure to solubilise the SWNTs by bonding long-chain molecules to its surface. Raw SWNTs were oxidised and shortened by prolonged sonication in a mixture of nitric and sulfuric acids. The carboxyl groups, which were presumably positioned at the edges of the tubes with a length of 300 nm, were converted to acid chloride groups by refluxing in thionyl chloride (containing some DMF) for 24 h. The DMF acts as a catalyst in the formation of acid chloride groups by SOCl$_2$.[28] Haddon et al. emphasised that the reaction of the SOCl$_2$-treated SWNTs with octadecylamine (ODA) in toluene was unsuccessful. The key to the preparation was the reaction of the tubes with pure molten ODA for an extended period of time. It is evident that severe reaction conditions are required for derivatisation of carbon nanomaterials.

In this investigation, we have studied the immobilisation of the rhodium/anthranilic acid complex onto fishbone carbon nanofibres. The reports by Haddon and co-workers and by Holy served as a basis to develop an immobilisation scheme. It will be shown that the Rh^{III}/anthranilic acid system immobilised on carbon nanofibres can indeed be synthesised. The complex is bonded to the fibres by an amide linkage of the CNF carboxyl groups and the amine functionality of anthranilic acid. The immobilised Rh^{III} complex is not active in the hydrogenation of cyclohexene. Reduction with NaBH$_4$ results in a very active catalyst that consists of extremely small rhodium particles. Milder activation procedures may lead to an active immobilised Rh^I complex.

Results

Infrared spectroscopy: Figure 1 shows the infrared spectra of CNF-U, CNF-OX, CNF-AA and of a physical mixture of
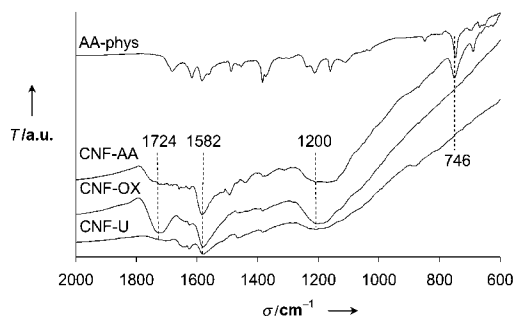

Figure 1. IR spectra of untreated (CNF-U), oxidised (CNF-OX), anthranilic-acid-treated (CNF-AA) carbon nanofibres, and of a physical mixture of anthranilic acid and CNFs (AA-phys).

carbon nanofibres and anthranilic acid (for explanations of the codes for the intermediate products and final catalysts see Table 1). To allow comparison, transmission levels of all spectra were kept approximately the same. It was established that, within the transmission window used, the intensity of the bands did not depend upon the transmission level of the spectra. Table 2 summarises the band assignments. The assignment of the bands of untreated fibres[29] and of oxidised

Table 1. Abbreviations for the intermediate products and the final immobilised catalysts.

Abbreviation	Description
intermediate products	
CNF-U	untreated fibres
CNF-OX	oxidised fibres
CNF-SOCl$_2$	SOCl$_2$-treated fibres
CNF-AA	anthranilic-acid-treated fibres
final catalysts	
RhAA/CNF(17)	dried for 17 h after SOCl$_2$ treatment
RhAA/CNF(17,BH)	dried for 17 h, reduction with NaBH$_4$
RhAA/CNF(5)	dried for 5 h after SOCl$_2$ treatment
RhAA/CNF(17,DMF)	dried for 17 h, reaction AA in DMF

Table 2. Assignments of IR absorptions found for CNF-U, CNF-OX, CNF-AA and a physical mixture of CNFs and anthranilic acid.

Wavenumber [cm^{-1}]	Assignment	References
1724	C=O stretching carbonyl + carboxyl	[30, 31, 34, 36]
1633	adsorbed water	[30, 31]
1582	aromatic ring stretching	[31, 34, 35]
1384	nitrate	[32, 33]
1200	C–C stretching	[31, 34]
746	aromatic C–H bending anthranilic acid	[37]

fibres[13] have already been reported and discussed in separate papers. The oxidation of carbon nanofibres has been extensively discussed in reference [13]. With regards to the untreated fibres, the absorptions at approximately 1630 and at 1384 cm^{-1} are attributed to adsorbed water and nitrate, respectively, on the KBr and can be discounted.[30–33] The minimum at 1582 cm^{-1} originates from an aromatic ring vibration, while the broad 1200 cm^{-1} absorption is attributed to the C–C stretching vibration.[31, 34, 35] Upon oxidation, an additional band appears at 1724 cm^{-1}. This peak originates from the C=O stretching vibration of carboxyl and/or carbonyl groups.[30, 31, 34, 36] Furthermore, the intensity of the 1200 cm^{-1} absorption intensifies as a result of CO stretching and OH bending vibrations that occur in this region.[34] The intensity of the 1582 cm^{-1} band also increases because, upon oxidation, symmetry restrictions are relieved for more aromatic rings.[29]

A comparison of the IR spectrum of a physical mixture of anthranilic acid and CNFs (AA-phys) with that of CNF-AA indicates that, as a result of the strong IR absorbance of CNFs, many bands visible in the spectrum of pure AA diminish, shift or even disappear upon mixing with carbon nanofibres. Therefore, the aromatic C–H bending mode at 746 cm^{-1} (indicative for four adjacent H atoms[37]) occurring in the

spectrum of CNF-AA appears to be the best indication for the presence of anthranilic acid on the surface of the CNFs. In addition, other absorptions are visible in the spectrum that can be attributed to anthranilic acid. Furthermore, in the spectrum of CNF-AA, the carboxyl C=O stretching vibration at 1724 cm^{-1} of CNF-OX has almost disappeared, indicating that an amide bond between the carboxyl groups on the CNFs and the amine groups of anthranilic acid has been formed.

The spectrum of CNF-SOCl$_2$ (not shown) was identical to that of CNF-OX. The spectrum of the fibres that were treated with anthranilic acid in DMF showed only a weak band at 753 cm^{-1}. Furthermore, the C=O stretching vibration at 1724 cm^{-1} was only slightly diminished.

X-ray photoelectron spectroscopy (XPS): The process of immobilisation was also followed with XPS. Figure 2A and B shows the Cl$_{2p}$ and the N$_{1s}$ regions, respectively, of CNF-OX, CNF-SOCl$_2$, CNF-AA, and RhAA/CNF(5). Oxidised fibres do not contain chlorine; however, this element is clearly
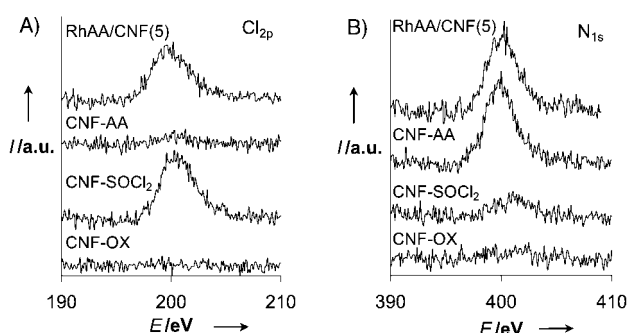
Figure 2. XPS spectra of A) the Cl$_{2p}$ region and B) the N$_{1s}$ region of CNF-OX, CNF-SOCl$_2$, CNF-AA, and RhAA/CNF(5).

present after treatment with SOCl$_2$. Upon reaction with anthranilic acid, the chlorine is removed, whereas after complexation of Rh (with RhCl$_3 \cdot 2H_2O$) it reappears on the surface of the CNFs. The presence of nitrogen on oxidised fibres is not detected with XPS. The small peak appearing in the spectrum of CNF-SOCl$_2$ can be attributed to small traces of DMF that is used during this synthesis step. The spectrum of CNF-SOCl$_2$ in Figure 2B has been obtained from CNF-SOCl$_2$ fibres that were dried for only five hours in a vacuum. The CNF-AA fibres clearly contain nitrogen, which remains present after complexation of Rh. Reduction with NaBH$_4$ or measurement of the catalytic activity does not affect the intensity of the N$_{1s}$ peak (spectra not shown).

The presence and the oxidation state of Rh was studied by monitoring the Rh$_{3d}$ peak. Figure 3 displays the results. The Rh$_{3d5/2}$ and Rh$_{3d3/2}$ transitions are both clearly visible. Only the Rh$_{3d5/2}$ peaks were used for further analysis. The spectrum of RhAA/CNF(17) shows one broad Rh$_{3d5/2}$ peak centred at 308.9 eV. Literature values for the Rh$_{3d5/2}$ peak in Rh$_2O_3$ and RhCl$_3$ are 308.2 – 308.8 eV and 310.1 eV, respectively.[38] Therefore, we can conclude that the Rh is in the trivalent oxidation state in this complex. Upon reduction of the RhAA/CNF(17) complex with NaBH$_4$ (denoted as RhAA/CNF(17,BH)), a second peak at ≈307.4 eV becomes the most
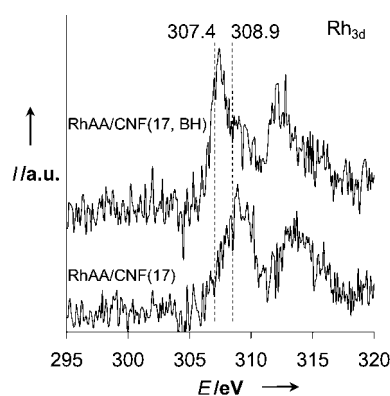
Figure 3. XPS spectra of the Rh_{3d} region of RhAA/CNF(17) and RhAA/CNF(17,BH).

Figure 4. XANES spectra of RhAA/CNF(17) (solid black) and RhAA/CNF(17,BH) (dotted black) together with Rh foil (solid grey) and Rh_2O_3 (dotted grey).

intense one and the peak at 308.9 eV is visible as a shoulder. As the $Rh_{3d5/2}$ peak for rhodium metal lies at 307.2 eV,[38] this new maximum indicates the presence of Rh^0. Clearly, a large portion of the Rh is in the zerovalent state after reduction with $NaBH_4$. A Rh^I complex would have given a peak at ≈ 308 eV.[38]

X-ray absorption fine structure (XAFS) spectroscopy

X-ray absorption near-edge structure (XANES): The X-ray absorption near-edge spectra of RhAA/CNF(17) and RhAA/CNF(17,BH) are shown in Figure 4 together with the data for Rh foil and Rh_2O_3. By comparison of the spectra of the RhAA/CNF(17) and RhAA/CNF(17,BH) samples with the reference compounds, information can be obtained about the oxidation state of the rhodium. The absorption edge of RhAA/CNF(17) is almost identical to that of Rh_2O_3. Thus, we can conclude that the Rh in RhAA/CNF(17) is in the trivalent oxidation state. No Rh–Rh interactions are present.

The position of the lower half of the absorption edge of RhAA/CNF(17,BH) is at a lower energy than that for RhAA/CNF(17) and closer to that of Rh foil. The increase in absorption intensity in this region of the absorption edge is typical of zerovalent rhodium. This suggests that part of the rhodium is in the zerovalent oxidation state.

Extended X-ray absorption fine structure (EXAFS) analysis: Figure 5 shows the experimental EXAFS data of RhAA/CNF(17) (Figure 5A) and RhAA/CNF(17,BH) (Figure 5C). The data quality is excellent. The signal-to-noise ratio at $k = 4.4$ Å^{-1} amounts to approximate-

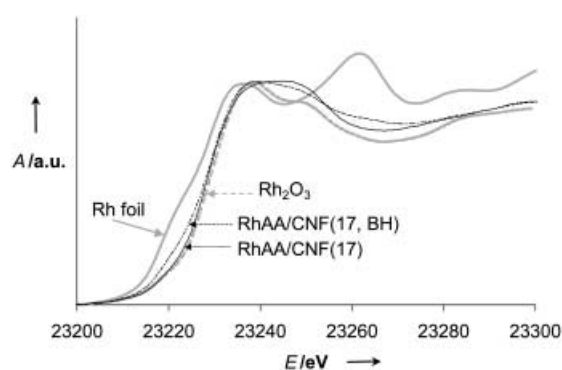ly 150 for RhAA/CNF(17) and 75 for RhAA/CNF(17,BH). It can clearly be seen that the EXAFS intensity of sample RhAA/CNF(17,BH) at larger values of k ($k > 10$ Å^{-1}) is higher than for RhAA/CNF(17), indicating the presence of a high Z scatterer.[39] The k^2 Fourier transform of the EXAFS data of RhAA/CNF(17) and RhAA/CNF(17,BH) are displayed in Figure 5B and D, respectively. Whereas the peak at 1.6 Å in both samples originates from low Z scatterers, such as oxygen, the peak at 2.4 Å in the uncorrected Fourier transform of the EXAFS data of RhAA/CNF(17,BH) is attributed to an Rh–Rh contribution. Also, the intensity of the first shell region at 1.6 Å is lower, indicating a change in coordination after reduction.

Figure 6A shows the Fourier transform (FT) of the experimental EXAFS data of RhAA/CNF(17) together with the FT of the total fit. The fit quality is excellent for the range
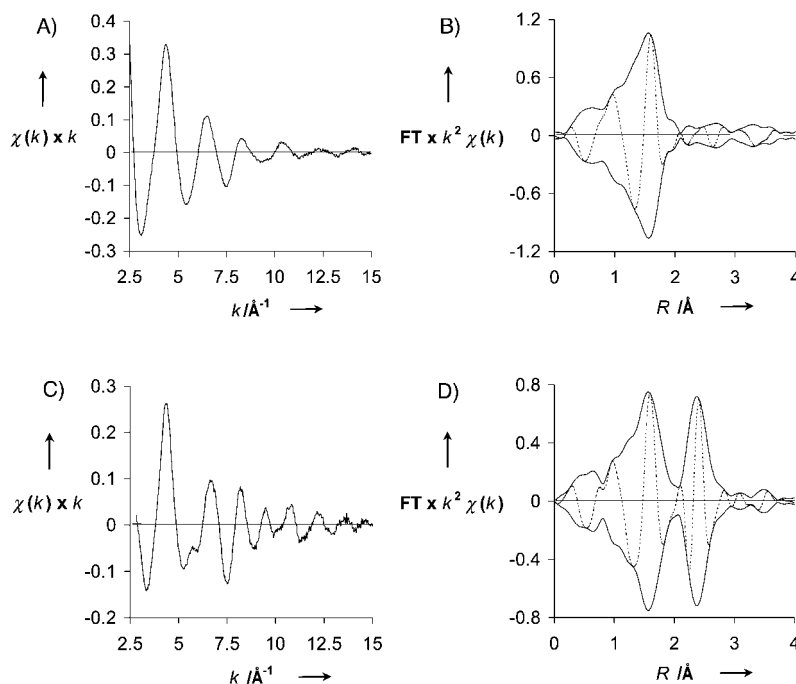

Figure 5. A) Experimental EXAFS spectrum of RhAA/CNF(17) (k^1 weighted). B) Corresponding uncorrected Fourier transform (k^2 weighted, $\Delta k = 2.7 – 15.9$ Å^{-1}). C) Experimental EXAFS spectrum of RhAA/CNF(17,BH) (k^1 weighted). D) Corresponding uncorrected Fourier transform (k^2 weighted, $\Delta k = 2.9 – 15.9$ Å^{-1}).

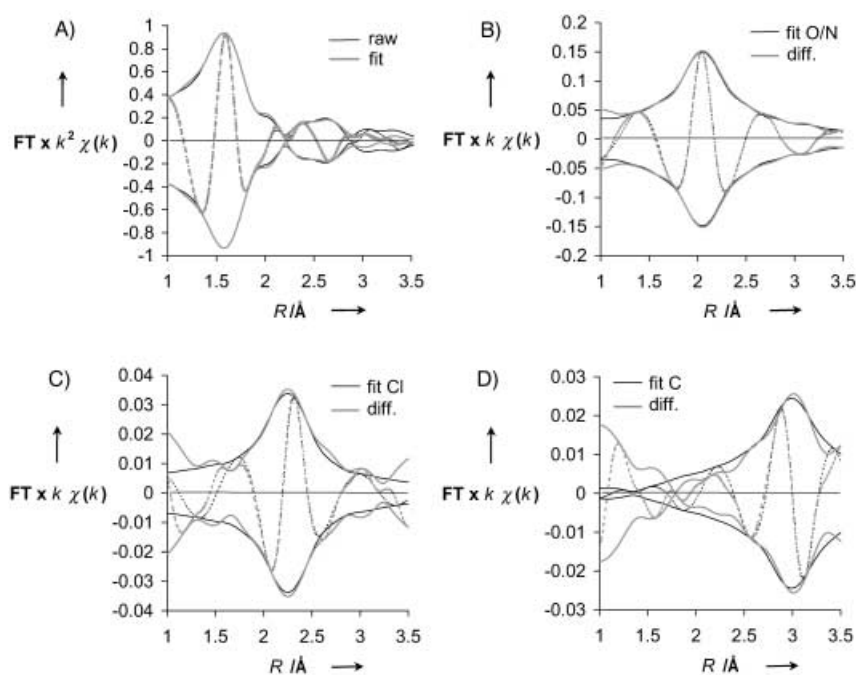Figure 6. Fit results of RhAA/CNF(17) ($\Delta k = 3.9 - 14$ Å^{-1}, $\Delta R = 1 - 2.8$ Å). A) Fourier transform of experimental EXAFS data and total fit (k^2 weighted, uncorrected). B) Rh–O fit and corresponding difference file (k^1 weighted, Rh–O phase-corrected). C) Rh–Cl fit and corresponding difference file (k^1 weighted, Rh–Cl phase-corrected). D) Rh–C fit and corresponding difference file (k^1 weighted, Rh–C phase-corrected).

of fits used ($\Delta R = 1 - 2.8$ Å). In RhAA/CNF(17), Rh–O/N, Rh–Cl and Rh–C contributions could be determined. The phase-corrected Fourier transforms of the fits of each individual contribution together with their corresponding difference files are shown in Figure 6B, C and D for the Rh–O/N, Rh–Cl and Rh–C contributions, respectively. The fit quality of each individual contribution is very good, indicating that reliable fit results for the weaker EXAFS contributions have been obtained as well. Table 3 presents the fit parameters of the EXAFS spectra resulting from the multiple shell fits in R space and the variances of the imaginary and absolute part of the fits for all catalysts. All variances obtained are well below 1%, indicating that excellent fit results for all catalysts have been acquired.[39] Furthermore, the calculated number of independent data points [see Eq. (3) later] is 14, showing that a fit with three shells is possible. Because the contributions of carbon, oxygen or nitrogen in RhAA/CNF(17) cannot be

easily distinguished, all these interactions were fitted with the Rh$_2$O$_3$ reference. The rhodium atom in the immobilised complex has five oxygen or nitrogen neighbours at a distance of 2.05 Å. The presence of carbon at such a distance is unlikely. One chlorine atom is also present in the coordination sphere of Rh at a distance of 2.28 Å. At a larger distance of 2.94 Å, three neighbours are fitted, which are most likely carbon atoms. No Rh–Rh interactions could be fitted.

The fit results of RhAA/CNF(17,BH) are also shown in Table 3. Again, very good results are obtained for the total fit and the three separate Rh–Rh, Rh–O and Rh–C contributions. There are 4.5 Rh neighbours situated at a distance of 2.68 Å. The coordination number of oxygen neighbours amounts to 3.4 at 2.05 Å. Finally, 1.6 C atoms are visible at a distance of 2.25 Å. The fit parameters of RhAA/CNF(5) displayed in Table 3 show that, besides oxygen and chlorine contributions ($N_O = 4.1$, $R_O = 2.07$, $N_{Cl} = 2.6$, $R_{Cl} = 2.28$), RhAA/CNF(5) contains some Rh–Rh interactions ($N = 2.0$, $R = 2.69$). A reasonable fit can also be obtained with less chlorine. RhAA/CNF(17,DMF) contains almost exclusively Rh–Rh interactions ($N = 8.2$, $R = 2.69$), but some Rh–O interactions are present as well ($N = 1.3$, $R = 2.05$).

It should be noted that with all catalysts, edge steps were obtained that were equal to the theoretical edge step for 1 wt% Rh on carbon. In other words, all catalysts indeed contain 1 wt% of Rh. The total discolouration of the water phase (containing the equivalent of 1 wt% Rh) after complexation of rhodium supports these observations.

Molecular modelling: The outcome of the EXAFS fit results of RhAA/CNF(17), namely the number and nature of

Table 3. Fit parameters of EXAFS spectra and variances of fits.[a]

Catalyst	Atom	N ±5%	R [Å] ±1%	$\Delta\sigma^2$ [Å^2] ±5%	ΔE_0 [eV] ±10%	k^2 Variance [%] Im	k^2 Variance [%] Abs
RhAA/CNF(17)	O/N	5.0	2.05	0.001	− 3.1	0.12	0.05
	Cl	1.0	2.28	0.004	4.4		
	C	2.9	2.94	0.003	− 10.6		
RhAA/CNF(17,BH)	Rh	4.5	2.68	0.006	9.9	0.25	0.12
	O	3.4	2.05	0.001	− 4.4		
	C	1.6	2.25	0.008	− 8.6		
RhAA/CNF(5)	Rh	2.0	2.69	0.006	7.0	0.06	0.03
	O	4.1	2.07	0.006	− 9.2		
	Cl	2.6	2.28	0.004	10.7		
RhAA/CNF(17,DMF)	Rh	8.2	2.69	0.000	5.6	0.10	0.04
	O	1.3	2.05	0.004	− 8.5		

[a] $\Delta k = 3.9 - 14$ Å^{-1}, $\Delta R = 1 - 2.8$ Å, k^2 weighted.

neighbours of Rh, were used as the input for the molecular modelling study. It was assumed that the rhodium is in the trivalent oxidation state and that, for reasons of charge compensation, both the carboxyl and the amide group of anthranilic acid are ionised. The result is shown in Figure 7; the carbon nanofibre structure is depicted on the left-hand side of the figure. Anthranilic acid is bonded to the fibre through an amide bond with a carboxyl group on the surface of the CNF. Rh is coordinated to anthranilic acid through one oxygen of the carboxyl group (of AA) and the nitrogen atom. In addition to one chloride anion, the coordination sphere of the rhodium atom is completed by three water molecules (the last synthesis step was performed in water). Thus, the Rh atom is in an

Figure 8. H_2 Flow and H_2 uptake curves of RhAA/CNF(17,BH).
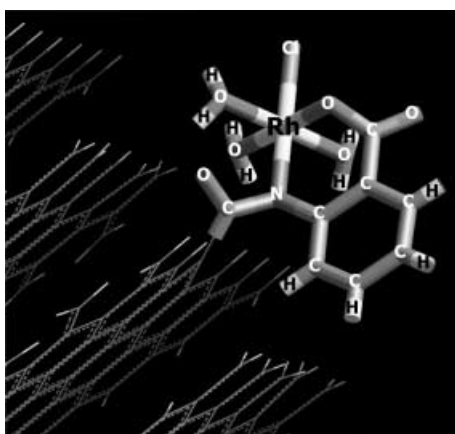

Figure 7. Outcome of the molecular modelling study of RhAA/CNF(17).

octahedral environment. Table 4 gives the distances of several atoms to the central Rh atom. For comparison, the EXAFS results have been included as well. The oxygen atoms of the three water molecules are situated at a distance of 1.9 Å. The oxygen atom of the carboxyl group of anthranilic acid is found at 2.0 Å, as is the AA nitrogen atom. Chloride resides at a distance of 2.3 Å. Three carbon atoms are found at distances of 2.8 Å (C of carboxyl group AA), 3.0 Å (carbon of benzyl ring) and 3.0 Å (C of carboxyl group CNF). These distances agree very well with the EXAFS results.

Table 4. Distances between Rh and several atoms in the molecular model of RhAA/CNF(17). The EXAFS results have been included for comparison.

| Atom | Modelling | | EXAFS | |
	No. of atoms	Distance [Å]	N	R [Å]
O_{H2O}	3	1.9 (3 ×) ⎫		
O_{carb}	1	2.0 ⎬	5.0	2.05
N	1	2.0 ⎭		
Cl	1	2.3	1.0	2.28
C	3	2.8, 3.0, 3.0	2.9	2.94

Catalytic measurements: The catalytic measurements resulted in a plot of the H_2 flow against time (see Figure 8 for RhAA/CNF(17,BH)). This curve was integrated to get an H_2 uptake pattern, which, in turn, was used to calculate the normalised initial activity (i.e., the activity at $t = 0$). The results are summarised in Table 5. Both RhAA/CNF(17) and RhAA/CNF(5) do not display any hydrogenation activity. The catalyst reduced with $NaBH_4$, on the other hand, is highly active. The activity of RhAA/CNF(17,BH) amounts to 1.1 mol H_2 $g_{cat}^{-1}h^{-1}$. RhAA/CNF(17,DMF) shows an intermediate activity of 0.3 mol H_2 $g_{cat}^{-1}h^{-1}$.

Table 5. Initial activities for the different catalysts.

Catalyst	Initial activity [mol H_2 $g_{cat}^{-1}h^{-1}$]
RhAA/CNF(17)	0.0
RhAA/CNF(5)	0.0
RhAA/CNF(17,BH)	1.1
RhAA/CNF(17,DMF)	0.3

Discussion

Infrared spectroscopy: The appearance of the aromatic C–H bending vibration of anthranilic acid at 746 cm^{-1} and the strong decrease in intensity of the C=O stretching band at 1724 cm^{-1} in the IR spectrum of CNF-AA strongly indicate that anthranilic acid has been bonded to the carboxyl groups of the oxidised carbon nanofibres through an amide linkage. Reaction of anthranilic acid through the carboxyl group is highly unlikely because it would result in an acyclic acid anhydride which is very unstable.[40] Unfortunately, no amide C=O stretching vibration could be observed. This band would be expected to be located at ≈1650 cm^{-1}.[24, 26, 27, 37] In this region, the adsorbed water peak and bands originating from anthranilic acid occur as well and, therefore, no clear statement concerning the presence or absence of this vibration can be made.

The IR spectrum of CNF-SOCl$_2$ is identical to that of oxidised fibres. No evidence for acid chloride groups could be found. However, it is possible that the acid chloride groups are not stable and that they are converted back to carboxylic acid groups under the influence of water vapour in the air. Another explanation could be that anthranilic acid reacts directly with the carboxyl groups of the CNFs under the conditions used (usage of pure molten AA). To investigate this, oxidised

carbon nanofibres were treated with pure molten anthranilic acid without prior treatment with SOCl$_2$. The IR spectrum of these CNFs is very similar to that of CNF-AA. In other words, the anthranilic acid 746 cm^{-1} band is clearly visible and the 1724 cm^{-1} C=O stretching vibration of the carboxyl group has almost disappeared. This result proves that anthranilic acid can react directly with the CNF carboxyl groups. This reaction was also investigated by Pittman et al.,[41] who treated polyacrylonitrile (PAN) carbon fibres oxidised with HNO$_3$ with tetraethylenepentamine at 190 °C. An esterification reaction between the carboxyl group of anthranilic acid and an hydroxyl group on the surface of the oxidised CNFs is also possible; however, this would not lead to a strong decrease in intensity of the 1724 cm^{-1} C=O stretching band. In conclusion, water-sensitive acid chloride groups may be formed on the surface of the CNFs, but their formation is not necessary to achieve the bonding of AA to carbon nanofibres.

X-ray photoelectron spectroscopy (XPS): The N$_{1s}$ XPS spectra show the appearance of nitrogen on the surface of the CNFs after reaction with anthranilic acid. This nitrogen atom is not removed by any of the further treatments that are performed with the CNF-AA fibres (complexation of Rh, catalytic reaction and/or reduction with NaBH$_4$), indicating that it must be tightly bound to the carbon nanofibre surface. XPS also shows that, after treatment with SOCl$_2$, the fibres should be dried under vacuum for a long period of time in order to remove all DMF from the surface of the fibres. The effect of traces of DMF on the surface of the CNFs is dealt with later in this section.

The XPS Cl$_{2p}$ results also provide valuable information on the subsequent immobilisation sequence. Chlorine appears on the surface of the fibres after reaction with SOCl$_2$ and disappears again after the bonding of anthranilic acid. This suggests that acid chloride groups have been formed that are subsequently used for the bonding of AA. If the acid chloride groups are unstable in air, the XPS Cl signal then probably originates from HCl that is formed during the decomposition reaction. After complexation of Rh, chlorine is present again, implying that this element is present near the rhodium.

As has previously been shown and discussed, the C$_{1s}$ peak did not change shape upon oxidation of the CNFs.[13] Furthermore, all other chemical modifications did not show a change in the C$_{1s}$ peak shape. This observation can be explained by taking account of the probing depth of XPS of ≈2 nm for carbon materials. This means that a large fraction of the carbon atoms detected by XPS are situated below the surface of the carbon nanofibres. These atoms are not modified and, hence, do not contribute to a change in the shape of the C$_{1s}$ peak.

X-ray absorption fine structure (XAFS) spectroscopy: The outcome of the analysis of the EXAFS data of RhAA/CNF(17) demonstrates that the central rhodium atom has six nearest neighbours (typical for Rh^{III}) and that one of these neighbours is a chlorine atom. Furthermore, the EXAFS fit reveals an interaction with three carbon atoms at a longer distance. The EXAFS results imply that, for reasons of charge

compensation of the Rh^{III}, the carboxyl group as well as the nitrogen atom of the former amine group of anthranilic acid are ionised. The three carbon atoms may originate from the benzyl ring of anthranilic acid or from the carbon nanofibre support.

The EXAFS data also shed more light on the structure of the NaBH$_4$-reduced catalyst RhAA/CNF(17,BH). Because no reduction prior to the EXAFS measurement was carried out, the result of the analysis of the EXAFS data indicates the presence of small rhodium particles that are partly oxidised. The particles probably have a core of rhodium metal surrounded by rhodium oxide. As the Rh atoms also interact with the carbon support, it is most likely that the rhodium particles are semi-spherical. Because the rhodium particles are partially oxidised, it is not possible to directly estimate the particle size from the coordination number. However, the particles should be small, because an interaction with the support is still observed and the catalyst displays a high hydrogenation activity. We roughly estimate the particle size to lie in the range 1.5 – 2 nm.

The complex RhAA/CNF(5) contains some Rh – Rh interactions. As this complex probably contains a mixture of different structures, a reliable interpretation of the EXAFS data cannot be given. The RhAA/CNF(17,DMF) catalyst consists of Rh particles that have an oxidised outer surface. These particles are fairly large: no interaction with the CNF support can be distinguished.

General discussion: All characterisation techniques agree very well with each other. IR spectroscopy showed the presence of an amide bond between the carboxyl groups on the surface of the carbon nanofibres and anthranilic acid, whereas the XPS N$_{1s}$ region showed the presence of tightly bound nitrogen on the CNF surface after attachment of AA. Furthermore, XPS showed that the rhodium in the as-synthesised RhAA/CNF(17) complex is in the trivalent state and that reduction with NaBH$_4$ leads to the formation of zerovalent Rh. The XANES results are in full agreement with these observations.

Although the EXAFS data provide very valuable information about the nature and number of neighbours of Rh and their separation, a structure is not easily visualised. Therefore, the molecular modelling program was used. The constructed model of RhAA/CNF(17) agrees very well with the EXAFS results. The six nearest neighbours have distances that are in agreement with the EXAFS data. More importantly, the three nearest carbon atoms in the model have an average distance that matches the EXAFS distance. As one of these carbon atoms belongs to the former carboxyl group of the carbon nanofibre, this is another strong indication for the covalent bonding of the complex to the fibres. The model also shows that, although the complex is closely bonded to the CNF surface and steric hindrance is expected, the Rh in the Rh/anthranilic acid complex is able to obtain a regular octahedral environment.

The catalytic data show that when the Rh in the Rh/anthranilic acid complex is in the trivalent oxidation state, no catalytic activity is observed. Only after formation of rhodium metal particles is the catalyst active in the hydrogenation of

cyclohexene. It is known that Rh[I] is able to perform the oxidative addition/reductive elimination cycle that is required for catalysis of hydrogenation reactions by metal complexes. Therefore, we attempted to reduce the Rh[III] in RhAA/CNF(17) to the univalent oxidation state by the action of NaBH$_4$. This reducing agent has already been used for this purpose with the polystyrene-immobilised Rh[III]–AA complex.[5] The XPS and XANES data have shown that a large part of the rhodium in RhAA/CNF(17,BH) has become Rh[0] after reduction. Clearly, the reduction of the Rh[III] to Rh[I] cannot be achieved with NaBH$_4$. Its reducing properties are probably too strong. Therefore, the activation of the immobilised Rh/anthranilic acid complex should be executed differently. One option could be the use of a milder reducing agent than NaBH$_4$. Another alternative might be to introduce the rhodium already as Rh[I] and not as Rh[III]. A risky reduction step would then be circumvented.

As was already demonstrated above with XPS, treatment of the oxidised fibres with SOCl$_2$/DMF results in the presence of DMF on the fibres if the drying procedure under vacuum is carried out for only a few hours. The final complex RhAA/CNF(5) contains some Rh–Rh interactions. Likewise, the attempt to use a solution of anthranilic acid in DMF for the attachment of this ligand to the fibres, ultimately leads to the formation of large Rh particles (RhAA/CNF(17,DMF). As Rh[0] is formed in both cases, we postulate that zerovalent rhodium is formed as a result of the reducing properties of DMF. When DMF is present on the surface of the carbon nanofibres, some or all of the rhodium chloride is reduced to Rh[0]. Only when DMF is totally removed, which presumably was achieved with the RhAA/CNF(17) complex after evacuation for 17 h, the rhodium can fully coordinate to anthranilic acid.

Conclusion

The immobilisation of Rh/anthranilic acid onto fishbone carbon nanofibres was executed by means of 1) surface oxidation of the fibres, 2) conversion of the carboxyl groups into acid chloride groups, 3) attachment of anthranilic acid and 4) complexation to rhodium(III). We have demonstrated that anthranilic acid bonds to the CNFs by an amide linkage with carboxyl groups that are present after surface oxidation of the fibres. The immobilised anthranilic acid coordinates to rhodium through the nitrogen atom and the carboxyl group. The coordination sphere of the trivalent Rh atom is further occupied by three water molecules and a chloride ion. To the best of our knowledge, this is the first example of a metal–ligand complex immobilised by covalent bonding on carbon nanofibres or carbon nanotubes.

The as-synthesised complex is not active in the hydrogenation of cyclohexene. Therefore, we reduced the rhodium with sodium borohydride in order to obtain monovalent rhodium. Rh[I] can participate in the oxidative addition/reductive elimination cycle that is required for catalysis. However, the reduction procedure with NaBH$_4$ results in the formation of small rhodium particles with an estimated diameter of 1.5–2 nm on the CNFs. The hydrogenation

activity of these particles is very high. We conclude that another activation procedure for the immobilised Rh/anthranilic acid system must be designed, for example, reduction with a milder reducing agent or complexation of the rhodium in the Rh[I] state. Solvents with reducing properties should be used carefully during the immobilisation sequence. We have shown that traces of DMF on the surface of the carbon nanofibres already results in the formation of some zerovalent rhodium. The use of anthranilic acid in DMF also yields rhodium metal particles. The formation of acid chloride groups by the action of SOCl$_2$ is not necessary to bring about the bonding of anthranilic acid to the CNFs. Under the conditions used, anthranilic acid can react directly with the carboxylic groups of the fibres.

Experimental Section

Growth of fishbone carbon nanofibres: Carbon nanofibres of the fishbone type were produced by catalytic decomposition of CH$_4$ on a Ni/Al$_2$O$_3$ catalyst.[42–45] The Ni/Al$_2$O$_3$ catalyst with 30 wt % Ni metal loading was synthesised by the deposition–precipitation technique:[46] alumina (Alon-C, Degussa) was suspended in an acidified aqueous solution of nickel nitrate (Acros, 99%) and diluted ammonia was injected over a period of 2 h at room temperature under vigorous stirring until the pH had reached a value of 8.5. The mixture was stirred overnight, and the resulting the suspension was filtered, washed and dried at 120 °C. Finally, the catalyst was calcined at 600 °C in stagnant air for 3 h.

For the production of fishbone CNFs, the 30 wt % Ni/Al$_2$O$_3$ catalyst (0.5 g) was reduced at 600 °C in 14% H$_2$/N$_2$ (flow rate 350 mL min^{-1}) in a vertical tubular reactor (diameter 3 cm) for 2 h. After decreasing the temperature to 570 °C, methane (50% in N$_2$, flow rate 450 mL min^{-1}) was passed through the catalyst bed for 6.5 h. The yield of fibres amounted to approximately 12 g.

Immobilisation of Rh/anthranilic acid onto fishbone carbon nanofibres: Scheme 1 illustrates the experimental procedures used for the immobilisation of Rh/anthranilic acid onto fishbone CNFs: 1) The carbon nanofibres
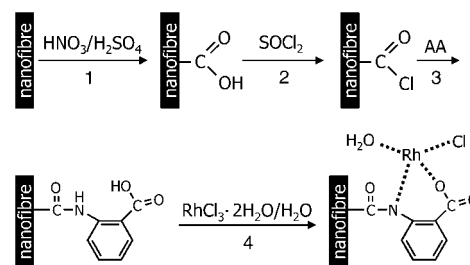
Scheme 1. Procedures used for the immobilisation of Rh/anthranilic acid on fishbone carbon nanofibres.

were first oxidised in a mineral acid mixture in order to create carboxyl groups on the surface and to remove the original Ni/Al$_2$O$_3$ growth catalyst. 2) These carboxyl groups were converted into acid chloride groups by the action of thionyl chloride and DMF. 3) Anthranilic acid was bonded to the fibres by reaction with these acid chlorides. 4) Subsequently, the immobilised anthranilic acid was complexed to rhodium by refluxing the fibres in an aqueous solution of rhodium(III) chloride. Finally, the Rh/anthranilic acid complex was reduced with sodium borohydride (procedure not shown in Scheme 1). Steps 2 and 3 (generation of acid chloride groups and attachment of anthranilic acid) were carried out under a nitrogen atmosphere with standard Schlenk techniques.

The fishbone carbon nanofibres were oxidised in a mixture of concentrated nitric and sulfuric acid. The CNFs (5 g) were boiled under reflux in HNO$_3$/H$_2$SO$_4$ 1:1 for 30 min (80 mL; HNO$_3$: Lamers & Pleugers, 65%, pure;

H_2SO_4: Merck, 95–97%, p.a.). Upon cooling and dilution with demineralised water, the suspension was filtered over a Teflon membrane filter (pore diameter of 0.2 μm), washed with demineralised water until the washings showed no significant acidity and dried at 120 °C for 16 h.

Oxidised fibres (3 g) were treated with $SOCl_2$/DMF (50:1, 50 mL) by boiling under reflux for 24 h in a N_2 atmosphere ($SOCl_2$: Acros, >99.5%; DMF: Merck, p.a.). After cooling, the reaction mixture was decanted from the fibres, which were dried under vacuum at 40 °C for 5 h. Another batch of fibres was dried under vacuum for 17 h at room temperature to make sure that all DMF was removed from the $SOCl_2$-treated fibres.

Anthranilic acid (20 g; Acros, >98%) was dried by vacuum suction at 40 °C for 2 h and transferred under N_2 to the $SOCl_2$-treated fibres. This mixture was kept at a temperature above the melting point of anthranilic acid (144–148 °C) for 96 h. Upon cooling, the resulting purple liquid suspension was filtered over a Teflon membrane filter (pore diameter of 0.2 μm), thoroughly washed with ethanol, and dried under vacuum at room temperature for 17 h. The $SOCl_2$-treated fibres were also treated with a solution of anthranilic acid in DMF. The fibres were boiled under reflux for 96 h in a 1M solution of dried anthranilic acid in molsieve-dried DMF (20 mL). These fibres were washed with DMF and treated identically in subsequent experiments.

Anthranilic acid-reacted fibres (2 g) were dispersed in demineralised water (30 mL), $RhCl_3 \cdot 2H_2O$ (48 mg, 0.2 mmol) was added, and the suspension was boiled under reflux for 72 h. Upon cooling, the Rh-loaded fibres (max. 1 wt%) were separated from the colourless water fraction by filtration. The fibres were washed with demineralised water and dried under vacuum at room temperature for 17 h.

Reduction of the immobilised Rh/AA complex was carried out by dispersing Rh/AA/CNFs (1 g) in ethanol (10 mL; Merck, p.a.) and by adding $NaBH_4$ (55 mg; Alfa, 99%) and ethanol (10 mL). The evolution of gas indicated an immediate reaction. After stirring for 30 minutes at room temperature, the reduced catalyst was filtered from the colourless solution, washed with ethanol and dried under vacuum at room temperature for 17 h.

Characterisation: Characterisation of the samples was carried out by infrared spectroscopy (IR), X-ray photoelectron spectroscopy (XPS), X-ray absorption fine structure (XAFS) spectroscopy, and by molecular modelling.

Infrared spectroscopy: Transmission IR spectra were recorded on a Perkin–Elmer 2000 spectrometer equipped with an air dryer to remove the water vapour and carbon dioxide. A total of 100 scans were co-added at a resolution of 8 cm^{-1} and a boxcar apodisation. Samples were prepared by thoroughly mixing a small amount of ground nanofibres with pre-dried KBr. Tablets were pressed at 4 tons cm^{-2} in a vacuum for 2 min. The concentrations of the nanofibres ranged from 0.1–1‰ (m/m). All transmission spectra were baseline corrected.

X-ray photoelectron spectroscopy (XPS): The XPS data were obtained with a Vacuum Generators XPS system and a CLAM-2 hemispherical analyser for electron detection. Non-monochromatic Al$_{K\alpha}$ X-ray radiation was obtained by means of an anode current of 20 mA at 10 keV. The pass energy of the analyser was set at 20 eV.

Because of the overlap of the Rh$_{3d}$ signal with the broad C$_{1s}$ peak, the C$_{1s}$ signal of CNF-AA was subtracted from the C$_{1s}$/Rh$_{3d}$ peak of the rhodium-loaded catalysts, resulting in the isolation of the Rh signal. It was ascertained that the error in the intensity of the subtracted spectrum at the position of the maximum of the C$_{1s}$ peak was not more than the intensity of the Rh signal and that the baseline exhibited zero intensity after subtraction.

X-ray absorption fine structure (XAFS) spectroscopy

XAFS data collection: XAFS spectra at the Rh$_K$ edge (23 220 eV) were obtained at the HASYLAB (Hamburg, Germany) synchrotron beamline X1.1, which was equipped with a Si(311) double crystal monochromator. The monochromator was detuned to 50% of the maximum intensity to minimise the presence of higher harmonics. All measurements were performed in the transmission mode with ionisation chambers filled with an Ar/N_2 mixture to have an absorbance of 20 and 80% in the first and the second ionisation chamber, respectively.

The CNF samples (300 mg) were pressed into self-supporting wafers and mounted into an in-situ EXAFS cell equipped with Be windows.[47] Because

of the low concentration of Rh (1 wt%) and the low absorption by carbon, the calculated edge step was about 0.2. The Rh_2O_3 and $RhCl_3$ reference compounds (Aldrich, 99.8% and 98%, respectively) were diluted with boron nitride (Alfa, 99.8%) and pressed into self-supporting wafers (calculated edge step 1). The rhodium reference foil (Aldrich, 99.9%, 25 μm thickness) was mounted on the sample holder with Kapton tape. The EXAFS cell was flushed with purified and dried He for 15 minutes and cooled down to liquid nitrogen temperature prior to measurement.

XAFS data processing: Extraction of the EXAFS data from the measured absorption spectra was performed with the XDAP code developed by Vaarkamp et al.[48] Two or three scans were averaged and the pre-edge was subtracted by means of a modified Victoreen curve.[49] The background was subtracted by means of cubic spline routines with a continuously adjustable smooth parameter.[39, 50] Normalisation was performed by dividing the data by the height of the absorption edge at 50 eV, leading to normalised EXAFS data.

EXAFS phase-shifts and backscattering amplitudes: Data for phase shifts and backscattering amplitudes were obtained from the reference compounds: Rh foil for Rh–Rh, $RhCl_3$ for Rh–Cl, and Rh_2O_3 for Rh–O, Rh–C and Rh–N contributions.[39] Table 6 gives the crystallographic data and the forward and inverse Fourier transform ranges used to create the EXAFS references. Both the reference spectra and the samples were measured at liquid nitrogen temperature. This means that no temperature effect has to be included in the difference in Debye–Waller factor ($\Delta\sigma^2$) between sample and reference as obtained in the EXAFS data analysis.

Table 6. Crystallographic data and the forward and inverse Fourier transform (FT) ranges used to make the EXAFS references.

Atom pair	Ref. compd	Ref.	N^{ref}	R^{ref} [Å]	k^n	Forward FT ΔK [Å^{-1}]	Inverse FT ΔR [Å]
Rh–Rh	Rh foil	[51]	12	2.69	3	2.7–22.7	1.4–3.1
Rh–O	Rh_2O_3[a]	[52]	6	2.05	1	3.7–16.3	0.0–2.3
Rh–Cl	$RhCl_3$	[53]	6	2.30	1	3.1–18.0	0.0–2.9

[a] It was established with XRD that the Rh_2O_3 was in the hexagonal modification.

R space fitting, difference file technique and weight factor k^n: The EXAFS data-analysis program XDAP allows one to perform multiple-shell fitting in R space by minimising the residuals between both the magnitude and the imaginary part of the Fourier transforms of the data and the fit. R space fitting has important advantages compared to the generally applied fitting in k space and is extensively discussed in a recent paper by Koningsberger et al.[39]

The difference file technique was applied together with phase-corrected Fourier transforms to resolve the different contributions in the EXAFS data.[39] The difference file technique allows one to optimise each individual contribution with respect to the other contributions present in the EXAFS spectrum. If the experimental spectrum is composed of different contributions then Equation (1) is valid:

$$\text{Exp.Data} = \sum_{i=1}^{N} (\text{Fit})_i \tag{1}$$

whereby (Fit)$_i$ represents the fitted contribution of coordination shell i. For each individual contribution then Equation (2) should then logically be valid:

$$(\text{Fit})_j = \text{Exp.Data} - \sum_{i=1 \text{ and } i \neq j}^{N} (\text{Fit})_i \tag{2}$$

The right-hand side of this equation is further denoted as the difference file of shell j. A good fit is only obtained if the total fit and each individual contributing coordination shell correctly describe the experimental EXAFS and the difference file, respectively. In this way not only the total EXAFS fit, but also the individual fits of all separate contributions can be determined reliably.

Both high Z (e.g. metal–metal) and low Z (e.g. metal–oxygen) contributions are present in the EXAFS data collected on metal complexes dispersed on supports of a high surface area. The low Z contributions may arise from the ligands and/or from the support. A k^3 weighting emphasises

the high Z contributions to the spectrum, since high Z elements have more scattering power at high values of k than low Z elements. However, the use of a k^3-weighted EXAFS spectrum or Fourier transform makes the analysis much less sensitive to the presence of low Z contributions in the EXAFS data. In this study, the EXAFS fits have been checked by applying k^1, k^2 and k^3 weightings in order to be certain that the results are the same for all weightings.

Number of independent data points, variance and statistical significance: The number of independent data points (N_{indp}) was determined as outlined in the "Reports on Standard and Criteria in XAFS Spectroscopy" [Eq. (3)].[54]

$$N_{indp} = \frac{2 \Delta k \Delta R}{\pi} + 2 \qquad (3)$$

The variances of the magnitude and imaginary part of the Fourier transforms of fit and data were calculated according to Equation (4):

$$\text{Variance} = \frac{\int [k^n \{FT_{model}^n(R) - FT_{exp}^n(R)\}]^2 \, dR}{\int [k^n (FT_{exp}^n(R))]^2 \, dR} \times 100 \qquad (4)$$

In this study the statistical significance of a contribution has been checked by a comparison of the amplitude of (Fit)$_j$ with the noise level present in the difference file (the noise in the difference file is essentially the same as the noise in the experimental data).

Molecular modelling: Molecular modelling was executed with the force-field based program Cerius^2. The universal force-field routine was used. A (part of a) carbon nanofibre was simulated by taking several unit cells of graphite.

Catalytic test experiments: The catalytic activity of the immobilised Rh complexes in the hydrogenation of cyclohexene was tested in a semi-batch slurry reactor, operated at a constant pressure of 1200 mbar H$_2$. The thermostated, double-walled reaction vessel was equipped with vertical baffles and a gas-tight stirrer with a hollow shaft and blades for gas recirculation. The stirrer was operated at 2000 rpm. During the reaction, the hydrogen consumption was automatically monitored by a mass flow meter. It was assured that, under the conditions used, the rate of dissolution of H$_2$ in the solvent was higher than the maximum measurable rate of H$_2$ uptake.

In a typical experiment, the reaction vessel was filled with catalyst (100 mg) and ethanol (100 mL; Merck p.a.). The reactor was then thermostated at 25 °C, evacuated, filled with H$_2$, and pressurised. The reaction was started by injection of 1 mL cyclohexene (Acros 99 %) with a syringe.

Acknowledgements

[1] C. U. Pittman, Jr. in *Comprehensive Organometallic Chemistry, Vol. 8* (Eds.: G. Wilkinson, F. G. A. Stone, E. W. Abel), Pergamon, Oxford, **1982**, p. 553.

[2] F. R. Hartley, *Supported Metal Complexes*, Reidel, Dordrecht, **1985**.

[3] Yu. I. Yermakov, L. N. Arzamaskova, *Stud. Surf. Sci. Catal.* **1986**, *27*, 459.

[4] A. Choplin, F. Quignard, *Coord. Chem. Rev.* **1998**, *180*, 1677.

[5] N. L. Holy, *Tetrahedron Lett.* **1977**, *42*, 3703.

[6] N. L. Holy, *Fundam. Res. Homogeneous Catal.* **1979**, *3*, 691.

[7] N. L. Holy, *CHEMTECH* **1980**, 366.

[8] O. N. Efimov, M. L. Khidekel', V. A. Avilov, P. S. Chekrii, O. N. Eremenko, A. G. Ovcharenko, *Russ. J. Gen. Chem. USSR* **1968**, *38*, 2581.

[9] V. A. Avilov, Yu. G. Borod'ko, V. B. Panov, M. L. Khidekel', P. S. Chekrii, *Kinet. Catal.* **1968**, *9*, 582.

[10] O. N. Efimov, O. N. Eremenko, A. G. Ovcharenko, M. L. Khidekel', P. S. Chekrii, *Bull. Acad. Sci. USSR, Div. Chem. Sci.* **1969**, 778.

[11] V. A. Avilov, M. L. Khidekel, O. N. Eremenko, O. N. Efimov, A. G. Ovcharenko, P. S. Chekry, *US patent* **1973**, 3 755 194.

[12] E. N. Frankel, J. P. Friedrich, T. R. Bessler, W. F. Kwolek, N. L. Holy, *J. Am. Oil Chem. Soc.* **1980**, 349.

[13] T. G. Ros, A. J. van Dillen, J. W. Geus, D. C. Koningsberger, *Chem. Eur. J.* **2002**, *8*, 1151.

[14] K. P. de Jong, J. W. Geus, *Catal. Rev.-Sci. Eng.* **2000**, *42*, 481.

[15] A. A. Keterling, A. S. Lisitsyn, V. A. Likholobov, A. A. Gall', A.S Trachum, *Kinet. Catal.* **1990**, *31*, 1273.

[16] Yu. Yu. Volodin, A. T. Teleshev, V. V. Morozova, A. V. Tolkachev, Yu. S. Mardashev, E. E. Nifantyev, *Russ. Chem. Bull.* **1999**, *48*, 899.

[17] Y. Zhang, H.-B. Zhang, G.-D. Lin, P. Chen, Y.-Z. Yuan, K. R. Tsai, *Appl. Catal. A* **1999**, *187*, 213.

[18] H. B. Kagan, T. Yamagishi, J. C. Motte, R. Setton, *Isr. J. Chem.* **1978**, *17*, 274.

[19] M. V. McCabe, M. Orchin, *Fuel* **1976**, *55*, 266.

[20] B. F. Watkins, J. R. Behling, E. Kariv, L. L. Miller, *J. Am. Chem. Soc.* **1975**, *97*, 3549.

[21] M. Fujihira, A. Tamura, T. Osa, *Chem. Lett.* **1977**, 361.

[22] L. Horner, W. Brich, *Liebigs Ann. Chem.* **1977**, 1354.

[23] J. C. Lennox, R. W. Murray, *J. Am. Chem. Soc.* **1978**, *100*, 3710.

[24] T. Atoguchi, A. Aramata, A. Kazusaka, M. Enyo, *J. Electroanal. Chem.* **1991**, *318*, 309.

[25] J. Liu, A. G. Rinzler, H. Dai, J. H. Hafner, R. K. Bradley, P. J. Boul, A. Lu, T. Iverson, K. Shelimov, C. B. Huffman, F. Rodriguez-Macias, Y.-S. Shon, T. R. Lee, D. T. Colbert, R. E. Smalley, *Science* **1998**, *280*, 1253.

[26] J. Chen, M. A. Hamon, H. Hu, Y. Chen, A. M. Rao, P. C. Eklund, R. C. Haddon, *Science* **1998**, *282*, 95.

[27] M. A. Hamon, J. Chen, H. Hu, Y. Chen, M. E. Itkis, A. M. Rao, P. C. Eklund, R. C. Haddon, *Adv. Mater.* **1999**, *11*, 834.

[28] J. S. Pizey in *Synthetic Reagents, Vol. 1* (Ed.: J. S. Pizey), Ellis Horwood, Chichester, **1974**, p. 321.

[29] T. G. Ros, A. J. van Dillen, J. W. Geus, D. C. Koningsberger, *ChemPhysChem* **2002**, *3*, 209.

[30] M. S. P. Shaffer, X. Fan, A. H. Windle, *Carbon* **1998**, *36*, 1603.

[31] "Colloids and Surfaces in Reprographic Technology": W. M. Prest, R. A. Mosher, ACS Symp. Ser. **1982**, *200*, 225.

[32] K. Nakamoto, *Infrared and Raman Spectra of Inorganic and Coordination Compounds*, 4th ed., Wiley, New York, **1986**, p. 124.

[33] U. Zielke, K. J. Hüttinger, W. P. Hoffman, *Carbon* **1996**, *34*, 983.

[34] P. Painter, M. Starsinic, M. Coleman in *Fourier Transform Infrared Spectroscopy, Applications to Chemical Systems, Vol. 4* (Eds.: J. R. Ferraro, L. J. Basile), Academic Press, Orlando, **1985**, p. 169.

[35] D. B. Mawhinney, V. Naumenko, A. Kuznetsova, J. T. Yates, *J. Am. Chem. Soc.* **2000**, *122*, 2383.

[36] H. P. Boehm, *Carbon* **1994**, *32*, 759.

[37] B. S. Furniss, A. J. Hannaford, P. W. G. Smith, A. R. Tatchell, *Vogel's Textbook of Practical Organic Chemistry*, 5th ed., Longman, London, **1989**, p. 254.

[38] J. F. Moulder, W. F. Stickle, P. E. Sobol, K. D. Bomben, *Handbook of X-ray Photoelectron Spectroscopy*, Perkin–Elmer Corporation (USA), **1992**, p. 117.

[39] D. C. Koningsberger, B. L. Mojet, G. E. van Dorssen, D. E. Ramaker, *Top. Catal.* **2000**, *10*, 143.

[40] M. A. Fox, J. K. Whitesell, *Organic Chemistry*, 2nd ed., Jones and Bartlett, Boston, **1997**, p. 629.

[41] C. U. Pittman, Jr., G.-R. He, B. Wu, S. D. Gardner, *Carbon* **1997**, *35*, 317.

[42] M. S. Hoogenraad, PhD Thesis, Utrecht University (NL), **1995**.

[43] M. S. Hoogenraad, M. F. Onwezen, A. J. van Dillen, J. W. Geus, *Stud. Surf. Sci. Catal.* **1995**, *101*, 1331.

[44] J. W. Geus, M. S. Hoogenraad, A. J. van Dillen in *Synthesis and Properties of Advanced Catalytic Materials* (Eds.: E. Iglesia, P. W. Lednor, D. A. Nagaki, L. T. Thompson), Materials Research Society Pittsburgh, Pittsburgh, **1995**, p. 87.

[45] W. Teunissen, PhD Thesis, Utrecht University (NL), **2000**.

[46] J. W.Geus, *Stud. Surf. Sci. Catal.* **1983**, *16*, 1.

[47] M. Vaarkamp, B. L. Mojet, F. S. Modica, J. T. Miller, D. C. Konings-berger, *J. Phys. Chem.* **1995**, *99*, 16067.

[48] Website: http://www.xsi.nl.

[49] M. Vaarkamp, I. Dring, R. J. Oldman, E. A. Stern, D. C. Konings-berger, *Phys. Rev. B* **1994**, *50*, 7872.

[50] J. W. Cook, Jr., D. E. Sayers, *J. Appl. Phys.* **1981**, *52*, 5024.

[51] R. W. G. Wyckhoff, *Crystal Structures*, *Vol. 1*, 2nd ed., Wiley, New York, **1963**, p. 10.

[52] J. M. D. Coey, *Acta Crystallogr. B* **1970**, *26*, 1876.

[53] H. Bärnighausen, B. K. Handa, *J. Less-Common Metals* **1964**, *6*, 226.

[54] D. C. Koningsberger, *Jpn. J. Appl. Phys.* **1993**, *32*, 877.

 0947-6539/02/0813-2878 $ 20.00+.50/0